Large-eddy simulation of passive-scalar mixing using multifractal subgrid-scale modeling

By G. C. Burton

1. Motivation and objectives

Among the most important hallmarks of hydrodynamic turbulence is its ability to efficiently mix scalar quantities that exert no dynamic effect on the evolution of the flow itself. Passive-scalar mixing by turbulent flow is important in a diverse range of engineering and scientific applications, such as heat transfer, dispersion of pollutants in the atmosphere, and chemical mixing in numerous industrial and biological processes. Turbulent mixing is of particular interest to the modeling of reacting flows, such as those occurring in jet, rocket or internal-combustion engines, where turbulence is known to mix reactants in an extremely rapid manner, and thereby influence both the rate and efficiency of the reactive process. Often computational models for reactive flows are parameterized by small-scale statistics of the scalar field, such as the scalar variance and flux, which are thought to directly influence the availability of the scalar for reactions occurring at the molecular level. The accurate determination of such parameters, in turn, depends on understanding the processes by which the scalar, generally introduced at large scales in the flow, is made available by the turbulence for use in these small-scale processes.

Over the past two decades significant research has examined the complex phenomenon of passive-scalar mixing by turbulent flow. Experimental work has provided much insight into turbulent mixing, but has often been limited by the difficulty of obtaining high-fidelity data from highly turbulent flows of the sort typically seen in nature and applications. Direct numerical simulation (DNS) of passive-scalar mixing, in which all dynamically significant scales in a given flow are explicitly calculated, has been used increasingly as a complementary means of exploring the turbulent mixing process (see, *e.g.*, Yeung *et al.* 2005, Overholt & Pope 1996). However, as with experimental work, DNS studies have been limited to modestly turbulent flows, even for the few researchers having – at best limited – access to the nation's most powerful computers. For the foreseeable future, however, the vast majority of practicing engineers and scientists, with little or no routine access to such computing capability, must look to other methods to simulate this important class of flows.

In this context, large eddy simulation (LES) has been proposed as a promising method to numerically simulate many turbulent flows. In LES, the large-scale features of a turbulent flow are calculated explicitly, while the small scales, which are presumably universal, are modeled. This reduces computational costs, since modeling the small scales is significantly less burdensome than explicitly calculating them. However, most current subgrid-scale models developed for use in LES fail to recover the detailed spatial structure of the stress and energy transfer fields of such flows. These factors, nevertheless, may be of particular importance for modeling processes that occur principally in the subgrid scales, such as kinetic-energy dissipation, scalar-energy dissipation and chemical reactions, as well as being significant for the evolution of the large scales as well.

Recently, Burton & Dahm (2005 *a,b*) have proposed multifractal modeling with backscatter limiting as a new high-fidelity approach to large-eddy simulation. In that work, the authors derived a physical model for the subgrid velocities $\mathbf{u}^{sgs}$ based on the multifractal

structure of the subgrid enstrophy field $\mathcal{Q}^{sgs}(\mathbf{x},t) = \frac{1}{2}\boldsymbol{\omega}^{sgs} \cdot \boldsymbol{\omega}^{sgs}(\mathbf{x},t)$. The resulting subgrid-scale model is then used to directly calculate the nonlinear term $\overline{u_i\, u_j}$ in the filtered Navier-Stokes momentum equation. When combined with physical backscatter limiting, the method has shown special promise because, at modest computational cost, multifractal modeling can recover the detailed spatial structure of the momentum and energy transfer fields in LES with high accuracy ($\rho \geq 0.99$).

Importantly, multifractal modeling may be applied to other under-resolved turbulence problems, such as the mixing of a passive scalar. The derivation of such a model was set out in Burton (2004), where the already-established multifractal structure of the scalar dissipation field $\chi^{sgs}(\mathbf{x},t)$ (see, *e.g.*, Frederiksen *et al.* 1997, Prasad *et al.* 1988) was used to derive a physical model for the subgrid scalar concentrations ϕ^{sgs} that permits direct calculation of the filtered product term $\overline{u_j\,\phi}$ in the filtered scalar transport equation. That work reported the results of *a priori* tests in which the passive-scalar model was compared against DNS data, and which concluded that the model recovered significant structural characteristics of the scalar flux and scalar energy production fields. It then reported initial results from large-eddy simulations indicating that the computational system ran stably and accurately over very-long time integration. In this report, further *a posteriori* tests are described in which multifractal modeling is employed in LES of passive-scalar mixing, where the scalar field is forced by a mean-scalar gradient or isotropically in Fourier space. The tests focus on two sets of simulations, one at Schmidt number $Sc = 1$, and a second at high Schmidt numbers $Sc \gg 1$. These tests indicate that multifractal modeling recovers significant characteristics of both regimes, previously observed in experimental and DNS studies.

2. Results

2.1. *Background: LES of passive-scalar mixing*

In general, the time evolution of a passive scalar ϕ in an incompressible turbulent flow is governed by an advection-diffusion equation given by

$$\frac{\partial\,\phi}{\partial t} + \frac{\partial}{\partial x_j}\,(u_j\,\phi\,) \;-\; D\,\frac{\partial^2}{\partial x_j \partial x_j}\;\phi \;=\; 0, \tag{2.1}$$

where D is a coefficient of scalar diffusivity. Unlike the Navier-Stokes equation for the turbulent flow itself, this equation is linear in ϕ, which suggests that the dynamical processes governing passive-scalar evolution might be more amenable to analysis. However, theoretical, experimental and computational work over the past two decades has indicated that turbulent scalar mixing is a complex phenomenon, which in significant respects differs from the dynamics of the underlying turbulence itself. While passive-scalar transport remains incompletely understood, such work has provided convincing evidence of persistent small-scale anisotropy in these scalar fields when subjected to large-scale anisotropic forcing, contrary to the traditional assumption of universal isotropy at small scales as proposed by Kolmogorov and Obukhov (see, *e.g.*, Warhaft 2000). Other issues, such as scalar energy spectra scaling in high Schmidt number flows remain hotly debated at present.

In contrast to DNS studies, large eddy simulations of passive scalar transport most often use a filtered version of (2.1) that is given by

$$\frac{\partial\overline{\phi}}{\partial t} + \frac{\partial}{\partial x_j}\,\overline{u}_j\,\overline{\phi} \;-\; D\frac{\partial^2\overline{\phi}}{\partial x_j \partial x_j} \;=\; -\,\frac{\partial}{\partial x_j}\,\sigma_j\,, \tag{2.2}$$

where the overbar $\overline{(\cdot)}$ represents a filter isolating the large scales in the flow, and where the subgrid-scalar stress term σ_j is given by

$$\sigma_j \;\equiv\; \overline{u_j\,\phi} \;-\; \overline{u}_j\,\overline{\phi}\,. \tag{2.3}$$

Equations (2.2) and (2.3) involve interactions between the resolved and subgrid velocities $\overline{u}_j$ and u_j^{sgs} on the one hand, and the resolved and subgrid passive-scalar field $\overline{\phi}$ and ϕ^{sgs} on the other, and require some form of modeling.

Most passive-scalar models draw on an eddy-diffusivity assumption that parallels the eddy-viscosity paradigm most frequently used in LES. In these approaches, σ_j of (2.3) is then related to the magnitude of the local scalar-strain rate field and transport is assumed to be oriented down this resolved gradient. Such an approach had been taken, for example, by Moin *et al.* (1991) in which an eddy-diffusivity model was implemented using a dynamic procedure. Physically-based models for passive-scalar mixing have been proposed only rarely. For example, Pullin (2000) proposed a subgrid-scalar model within the framework of the stretched-vortex method that provided reasonably accurate recovery of various integrated scalar quantities. However, no previously proposed subgrid-scalar model has been shown to recover the detailed spatial structure of the scalar-flux or scalar energy transfer field in a large-eddy simulation.

An alternative to (2.2)-(2.3) is to cancel the advection operator in (2.2) with the second term on the r.h.s of (2.3). This reduces all of the convective forces acting on the scalar field to the single filtered scalar flux term $\overline{u_j\,\phi}$. Thus, the filtered scalar transport equation can be written equivalently as

$$\frac{\partial\overline{\phi}}{\partial t} + \frac{\partial}{\partial x_j}\,\overline{u_j\,\phi} - D\frac{\partial^2\overline{\phi}}{\partial x_j\partial x_j} \;=\; 0\,, \tag{2.4}$$

where

$$\overline{u_j\,\phi} \;\equiv\; \overline{\overline{u}_j\,\overline{\phi}} + \overline{\overline{u}_j\,\phi^{sgs}} + \overline{u_j^{sgs}\,\overline{\phi}} + \overline{u_j^{sgs}\,\phi^{sgs}}\,. \tag{2.5}$$

Multifractal models for the subgrid velocities u_j^{sgs} and subgrid scalar concentrations ϕ^{sgs} may be then used to calculate directly the filtered scalar flux term appearing in (2.4) and (2.5). In multifractal modeling, the subgrid quantities are approximated as scaling operations on the smallest resolved scale Δ in the simulation, where $u_j^{sgs} \approx \mathcal{B}u_j^{\Delta}$ and $\phi^{sgs} \approx \mathcal{D}\phi^{\Delta}$, and where the proportionality constants $\mathcal{B}$ and $\mathcal{D}$ exhibit weak Reynolds-number dependence. The reader is referred to Burton (2004) and Burton & Dahm (2005*a*) for detailed derivations of the scalar and momentum closure models, respectively.

2.2. *Multifractal LES: computational method*

In order to test the accuracy of multifractal modeling for passive scalar transport, a series of large eddy simulations of passive scalar mixing by homogeneous isotropic turbulence were conducted in the presence of an imposed mean-scalar gradient. These simulations were configured to replicate several experimental studies that have examined passive scalar mixing by grid turbulence in the presence of a mean-scalar gradient (see, *e.g.*, Mydlarski & Warhaft 1998). The present simulations therefore were initialized with fluctuating velocity and scalar fields, each randomized as to phase, periodic in the cubic interval $I \equiv [-\pi, \pi]$. In one group of simulations both the velocity and scalar fluctuation fields were initialized with energy distributions consistent with a $\sim\; k^{-5/3}$ scaling. In other simulations the initial fluctuating scalar field was initialized as a double-delta distribution with values of 0 and 1, where the probability density function is given as $\beta(\phi) \equiv 0.5\,\delta(\phi - 0) + 0.5\,\delta(\phi - 1)$. This distribution gives an initial scalar energy field with scaling $E_\phi(k) \sim$

k^2. It was determined that both initial scalar fields produced similar final results with simulations integrated to a statistically stationary state.

For each simulation an initial mean scalar gradient $\boldsymbol{\alpha}$ was added to the initial fluctuating field, where the mean scalar field is given by

$$\langle\,\phi\,\rangle(\mathbf{x},t_o) = \alpha_j\, x_j\,. \tag{2.6}$$

In the present simulations, $\boldsymbol{\alpha} \equiv [0,0,1/2\pi]$ with the mean scalar field periodic in directions normal to the gradient. As the simulation progresses, the mean scalar gradient is maintained by fixing the boundary values of the mean scalar field consistent with its initial distribution in the non-periodic direction. The operator $\langle\,\cdot\,\rangle$ in (2.6) is therefore taken as an instantaneous average of the scalar field in planes normal to the gradient, so that the mean scalar field is a function only of the single coordinate direction x_k, and therefore varies, as in an actual experimental configuration, continuously in space and time.

Given this initial configuration, it is useful to consider a triple decomposition of the complete scalar field that is evolved in the simulation as

$$\phi(\mathbf{x},t) \equiv \underbrace{\langle\,\phi\,\rangle\,(\mathbf{x},t) + \overline{\phi'}(\mathbf{x},t)}_{\overline{\phi}(\mathbf{x},t)} + \phi^{sgs}(\mathbf{x},t), \tag{2.7}$$

where the resolved field $\overline{\phi}$ is comprised of a mean and resolved fluctuating scalar field, and where the remaining component, the subgrid fluctuation field ϕ^{sgs}, must be modeled. Consistent with (2.7), the fluctuating scalar field is then comprised of resolved and subgrid portions, as

$$\phi^{'}(\mathbf{x},t) \equiv \overline{\phi'}(\mathbf{x},t) + \phi^{sgs}(\mathbf{x},t). \tag{2.8}$$

Substituting (2.7) into (2.4) and (2.5) gives the resolved scalar evolution equation as

$$\frac{\partial\,\overline{\phi}}{\partial t} + \frac{\partial}{\partial x_j}\left(\overline{u_j\,\langle\phi\,\rangle} + \overline{u_j\,\phi'}\right) - D\frac{\partial^2\,\overline{\phi}}{\partial x_j \partial x_j} = 0 \tag{2.9}$$

Where the scalar field is homogeneous and isotropic, $\langle\phi\rangle = 0$ and (2.9) reduces to (2.4).

From (2.9) it is apparent that each component of the resolved scalar field in (2.7) contributes to the stress exerted on any given fluid element in the simulation. By multiplying (2.9) by $\overline{\phi}$ from (2.7), the scalar-energy evolution equation for the resolved scalar field takes the form

$$\frac{\partial}{\partial t}\frac{\overline{\phi}^2}{2} + \frac{\partial}{\partial x_j}\left[\overline{\phi}\left(\overline{u_j\,\langle\phi\,\rangle} + \overline{u_j\,\phi'}\right) - D\,\overline{\phi}\,\frac{\partial\overline{\phi}}{\partial x_j}\right] = \left(\overline{u_j\,\langle\phi\rangle} + \overline{u_j\,\phi'}\right)\frac{\partial\overline{\phi}}{\partial x_j} - D\,\frac{\partial\overline{\phi}}{\partial x_j}\,\frac{\partial\overline{\phi}}{\partial x_j}. \tag{2.10}$$

The spatial derivative on the l.h.s. of (2.10), which is in divergence form, does not contribute to the transfer of scalar energy between the resolved and subgrid scales. In addition, the last term on the r.h.s of (2.10) represents dissipation of resolved scalar energy, and is in general small for highly turbulent flows. Most of the scalar energy transferred between the resolved and subgrid scales, however, is the result of the production term in (2.10), given by

$$-\mathcal{P}^{\phi} = \left(\overline{u_j\,\langle\phi\rangle} + \overline{u_j\,\phi'}\right)\frac{\partial\overline{\phi}}{\partial x_j}\,. \tag{2.11}$$

Here, $\mathcal{P}^{\phi}$ represents energy transfer due to the interaction of the scalar flux term $\overline{u_j\,\phi}$ and the resolved scalar strain-rate field. Where $\mathcal{P}^{\phi} > 0$, scalar energy is transfered to the subgrid scales, while where $\mathcal{P}^{\phi} < 0$ scalar energy is transferred from the subgrid to the resolved scales.

2.3. *Order-based backscatter limiting.*

The multifractal passive-scalar model was implemented in the present LES studies in conjunction with the backscatter limiter discussed more fully in Burton & Dahm (2005*b*). This physically-based limiter controls aliasing and other numerical errors arising during a simulation by making small reductions to the magnitude of those inertial stresses responsible for the backscatter of energy from the subgrid into the resolved scales. Burton & Dahm (2005*b*) describe the application of a constant limiter $C_{\mathcal{B}}$ that reduces backscatter stresses by 15%, and show that this reduction does not substantially reduce the fidelity of the simulation. The method was shown to be effective in part because multifractal modeling recovers the spatial structure of the momentum and energy production fields with such high fidelity (with correlations $\rho \geq 0.99$), that small modifications to the backscatter stresses, by way of the limiter, do not appreciably impact simulation accuracy.

Burton (2004) proposed a modification to that methodology, by combining backscatter reduction with forward-scatter acceleration, where the magnitude of the modification is a function of the order of the individual terms in the Legendre polynomial expansion used to represent the nonlinear terms $\overline{u_i\,u_j}$. That paper noted that the most physically realistic results were obtained where polynomial terms up to second order were not limited, but where higher-order polynomial terms were limited in proportion to each term's respective order. Thus, for the present simulations, an order-based, combined backscatter/forward-scatter limiter was applied both to the nonlinear terms in the filtered Navier-Stokes equation and to all components of the product terms $\overline{u_j\,\phi}$ in the passive-scalar evolution equation.

2.4. *Multifractal LES of passive-scalar mixing: $Sc = 1$ case*

The multifractal model was first tested in a series of large eddy simulations at low Schmidt number $Sc = 1$ and coarse resolution $N = 32^3$ and compared against results of previously-reported experimental and DNS studies. The simulations were run to varying final times t_f where $20t_o \leq t_f \leq 80t_o$, and where t_o is the global eddy-turnover time. The velocity field was forced at each timestep by rescaling the largest waveforms $|k| \leq 2$ so that a constant energy was maintained in those wavemodes throughout the simulation. Statistical measures of the resolved scalar fluctuation field $\overline{\phi'}$ were taken after the system had reached stationarity at approximately $t \geq 6t_o$, at a frequency of $2t_o$ to provide statistically independent sampling of the flow field. At each timestep, the resolved scalar fluctuation field was obtained by subtracting the instantaneous plane-averaged mean scalar value $\langle\,\phi\,\rangle(\mathbf{x}, t_o)$ from the total resolved scalar field $\overline{\phi}(\mathbf{x}, t_o)$ consistent with (2.7). These values were then provided to the multifractal modeling subroutines to determine all terms within the decomposition of the scalar flux $\overline{u_j\,\phi}$ consistent with (2.7) and (2.9).

The first series of simulations were made at a low Schmidt number $Sc = 1$ and at several Taylor-scale Reynolds numbers Re_λ, to evaluate multifractal model performance at varying Reynolds numbers. Figure 1*(left)* compares a typical probability density function for the resolved scalar fluctuations $\overline{\phi'}$ at $Re_\lambda \approx 170$ *(solid)* with a Gaussian distribution *(dotted)* having the same mean and variance. It is apparent that the scalar concentration distribution is nearly Gaussian at this moderate Re_λ. The kurtosis of the LES distribution is approximately $\mathcal{K}^4 \approx 2.7$, indicating slightly sub-Gaussian characteristics, which

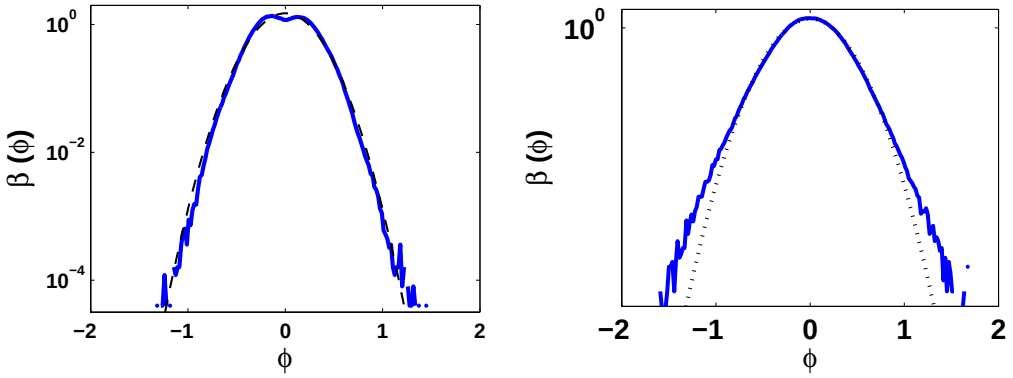

FIGURE 1. Probability distributions of the resolved scalar fluctuation field from LES with multifractal model at $Re_\lambda \approx 170$ (*left*), showing a sub-Gaussian distribution (with kurtosis $\mathcal{K}^4 \approx 2.7$), and at $Re_\lambda \approx 300$ (*right*), showing departure from Gaussian (with kurtosis of $\mathcal{K}^4 \approx 3.49$). These results suggest a trend to higher scalar intermittency at higher Reynolds number, consistent with the studies of Overholt & Pope (1996) and Gollub *et al.* (1991).

corresponds well with the results of Overholt & Pope (1996). By contrast, at a significantly higher Reynolds-number $Re_\lambda \approx 300$ in Fig. 1 *(right)* the scalar field displays higher intermittency, seen in the distribution tails, which depart significantly from the Gaussian. The kurtosis of the distribution is approximately $\mathcal{K}^4 \approx 3.49$, reflecting the higher intermittency. This finding is consistent with the experimental studies of Gullob *et al.* (1991), that found scalar distributions departing significantly from the Gaussian at Reynolds numbers higher than were examined by Overholt & Pope (1996).

A basic characteristic of the scalar energy distribution at low Schmidt number is a scalar energy distribution $E_\phi(k)$ exhibiting a scaling $\sim k^{-5/3}$ as predicted by Obukhov (1949) and Corrsin (1951). Figure 2 depicts the uncompensated and compensated scalar energy spectrum (*left and right, respectively*) from an LES using the multifractal model at $Re_\lambda \approx 170$. The compensated spectrum was normalized by $\langle E_\phi \rangle \langle \chi \rangle^1 \langle \epsilon \rangle^{1/3} k^{-5/3}$, in order to better highlight the scaling of the distribution. The graphic reflects scalar energy values averaged over the interval $20t_o - 70t_o$, after the simulation had reached a statistically stationary state. It is apparent that the simulation closely follows the $k^{-5/3}$ scaling predicted by Obukhov and Corrsin.

It has been shown both through experimental and numerical studies over the past decade that a passive-scalar field will display persistent anisotropy at inertial and dissipation range scales in otherwise isotropic turbulence when it is forced by a mean-scalar gradient. Such anisotropy manifests itself as a skewness in the distribution of the scalar fluctuation gradient $\nabla \phi'$ in the direction parallel to the mean-scalar gradient. It is thus instructive to evaluate how accurately multifractal modeling recovers this anisotropy. Figure 3 depicts the distribution of the resolved scalar fluctuation gradient component $\partial \phi'/\partial x_k$ parallel to the imposed mean scalar gradient *(solid)*, taken from an LES using multifractal modeling at $Re_\lambda \approx 200$. Approximately 25 statistically independent samples from the scalar field were taken over the time interval $20t_o - 70t_o$. This distribution is compared with a Gaussian distribution *(dotted)* having the same mean and variance as the scalar gradient distribution. The graphic shows that the scalar gradient distribution departs markedly from the Gaussian, with a skewness $\mathcal{S}^3 \approx 1.25$, close to the

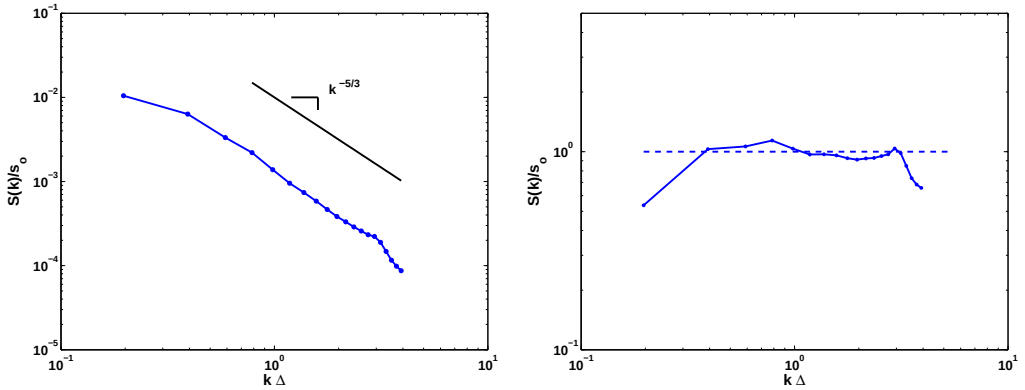

FIGURE 2. Averaged scalar energy spectra $E_\phi(k)$ uncompensated *(left)* and compensated by $\langle E_\phi\rangle\langle\chi\rangle^1\langle\epsilon\rangle^{1/3}k^{-5/3}$ *(right)* for LES at 32^3 and $Re_\lambda \approx 170$ and $Sc = 1$. The scalar field ϕ is forced by the mean scalar gradient given by (2.6). The scalar energy distribution closely follows the $k^{-5/3}$ scaling predicted by Obukhov and Corrsin.

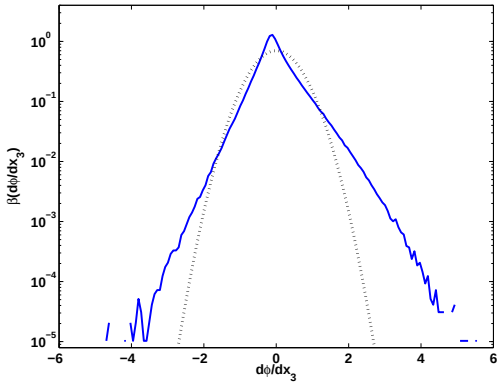

FIGURE 3. Filtered scalar fluctuation gradient $\partial\overline{\phi}/\partial x_j$ parallel to the mean scalar gradient, showing a skewness $\mathcal{S}^3 \approx 1.25$, close to the value seen in DNS and experimental studies at $Re_\lambda \approx 200$.

value $\mathcal{S}^3 \approx 1.3$ seen in DNS and experimental studies (see, *e.g.*, Overholt & Pope 1996; Mydlarski & Warhaft 1998) at similar Reynolds numbers.

The anisotropy manifesting itself in the skewness of the scalar gradient, as discussed above, results from "ramp-cliff" structures that appear in the scalar field directly from the turbulent mixing process. It has been shown previously that such structures naturally arise when adjoining eddies form saddle-points and separatrices in the velocity field, and thereby forcing the scalar field into cliff-like structures along the outflow directions (Antonia *et al.* 1986). These cliff-like structures are known to steepen with increasing Reynolds number. Where a mean-scalar gradient exists, even in otherwise isotropic turbulence, the process will skew the distribution of the scalar-fluctuation gradient in the direction parallel to the mean-scalar gradient. Figure 4 shows sample time signals from three locations within the simulation domain of the passive-scalar field during an LES at 32^3 using the multifractal model. Evidence of gradually steepening ramps near sharper cliff-like variations in the scalar values throughout the simulation reflects this important characteristic of the scalar mixing process.

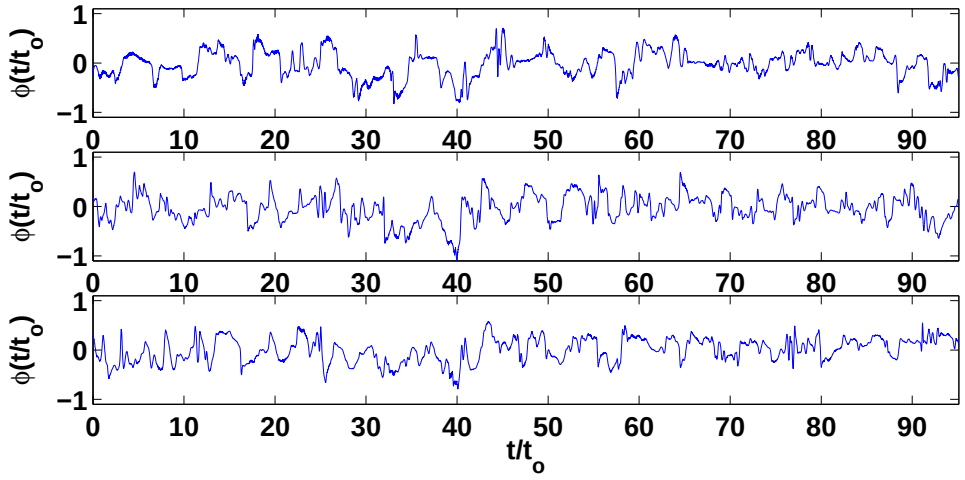

FIGURE 4. Timeseries signal for the filtered fluctuation scalar signal $\overline{\phi'}$ at three locations parallel to the imposed mean scalar gradient $\alpha_j\, x_j$ where $x_j = [-\pi, \pi]$, showing the ramp-cliff structures typical of a passive scalar field mixed by turbulent flow.

Two-dimensional extracts from a 64^3 LES depicted in Fig. 5, provide another view of this process. At Fig. 5 *left* is a contour plot of a single plane of data from the resolved scalar fluctuation field, with arrows superimposed over the scalar data indicating velocity streamlines. Careful examination of the graphic reveals cliff-like structures in the scalar field throughout the domain, with especially strong gradients in the center and lower left regions. Fig. 5 *right* is a detail from the center of the frame on the left, showing more closely the role played by eddy saddle-points and separatrices in forming the strong scalar cliff-like structure at frame center.

Recent DNS studies have also shown that passive-scalar mixing produces significantly higher intermittency in scalar-gradient quantities, such as scalar-energy dissipation, than the associated gradient quantities of the velocity field, such as kinetic-energy dissipation (Yeung *et al.* 2005). Figure 6 shows comparisons of the probability density functions of the normalized kinetic-energy dissipation field ε and the scalar-energy dissipation field χ from LES using the multifractal model at $N = 32^3$ and $Re_\lambda \approx 200$. It is apparent that the scalar dissipation field exhibits higher intermittency than the kinetic energy dissipation field, consistent with prior studies.

2.5. *Multifractal LES of passive-scalar mixing: $Sc \gg 1$ case.*

A second type of passive-scalar mixing occurs when the ratio of the kinematic viscosity to the molecular diffusivity of the passive scalar is much larger than $O(1)$. Such mixing occurs in a number of important applications, such as heat transport in liquids, pollutant and nutrient dispersion in the oceans, mixing of color dyes in flow visualization experiments, and in the mixing associated with various biological processes. The Schmidt numbers associated with these applications often reach in excess of $Sc \geq 10^2 - 10^3$ (Yeung *et al.* 2004). The dynamics of high Schmidt-number mixing, however, may depart in significant ways from scalar mixing when $Sc \approx O(1)$. For example, analytical work by Batchelor (1959) suggested that for $Sc \gg 1$, the scalar energy spectrum $E_\phi(k)$ should scale as k^{-1}, where viscous stress dominates the evolution of the turbulent flow, but convective scalar stress in (2.9) dominates the evolution of the passive-scalar field, *i.e.*,

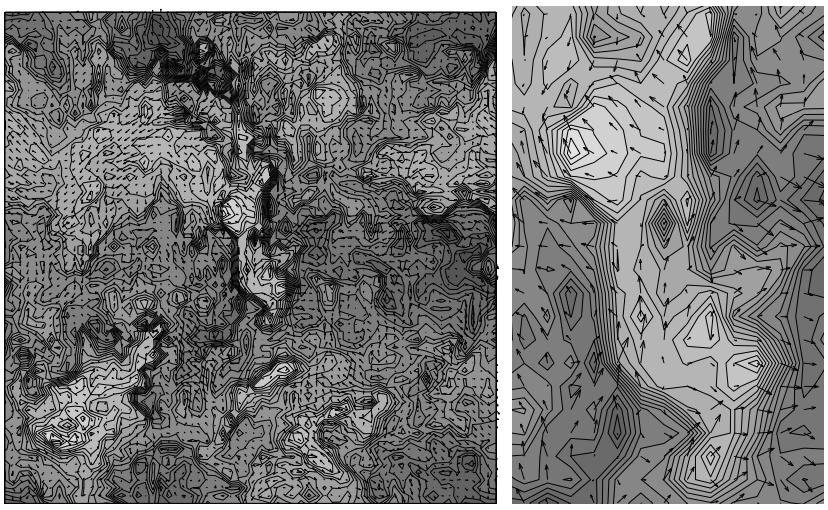

FIGURE 5. *(Left)* Contour plot of two-dimensional extract of resolved scalar fluctuation field $\overline{\phi'}(\mathbf{x})$ from 64^3 LES of passive-scalar mixing using the multifractal model at $Re_\lambda \approx 300$. The graphic shows distinctive "ramp-cliff" structures characteristic of passive-scalar mixing, especially apparent at center of frame and at lower left. *(Right)* Detail from center of frame at left showing relationship between saddle point of velocity field (indicated by arrows), and cliff portion of "ramp-cliff" structure in scalar concentration field.

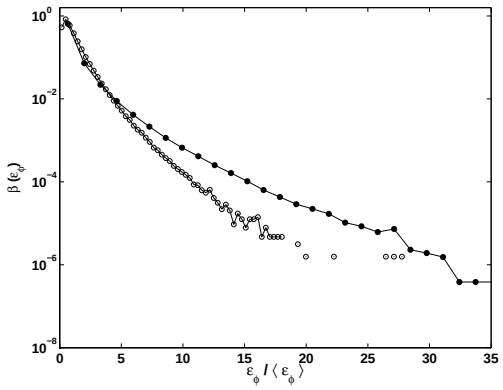

FIGURE 6. Comparison of distribution of normalized scalar dissipation field $\overline{\chi}/\langle\overline{\chi}\rangle$ *(dots)* versus normalized kinetic energy dissipation $\overline{\varepsilon}/\langle\overline{\varepsilon}\rangle$ *(circles)*, from LES with multifractal model at $Re_\lambda \approx 200$ and $Sc = 1$, showing significantly higher intermittency in the scalar dissipation field. Results are consistent with DNS studies of Yeung *et al.* (2005).

in the so-called "viscous-convective" range. This implies that there must be a large scale separation between the Kolmogorov scale η and the inner scalar length-scale $\eta_{\mathcal{B}}$, *i.e.,* where $\eta \gg \eta_{\mathcal{B}}$. Prior studies, however, have provided only mixed support for the existence of k^{-1} scaling in the viscous-convective region. For example, experimental work by Miller & Dimotakis (1995) found no evidence of k^{-1} scaling, at least for the case of a high Reynolds number shear flow with $Sc \approx 2000$. DNS studies of the high Schmidt-number regime, for example by Yeung *et al.* (2002, 2005), however, have supported the existence of k^{-1} scaling, but have been limited by resolution requirements to simulations where the velocity field is modestly turbulent, with $Re_\lambda \leq 38$. As a result, the characteristics of

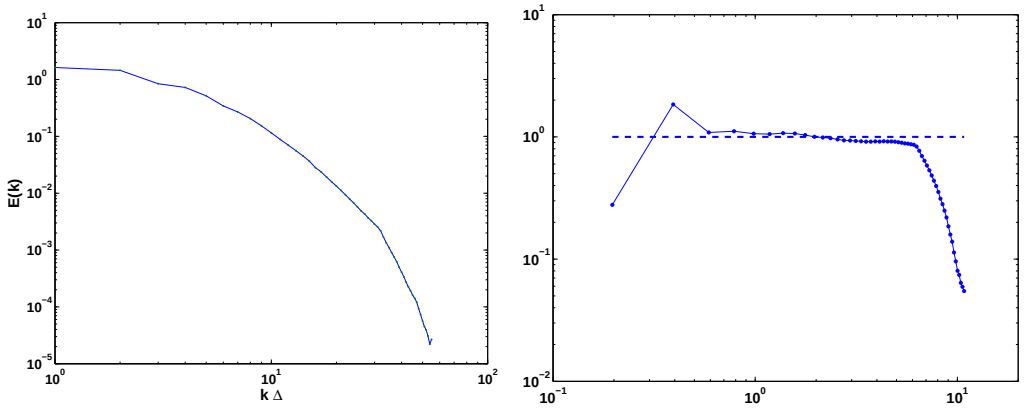

FIGURE 7. Energy spectrum $E(k)$ *(left)* and scalar energy spectrum *(right)* compensated by $\langle E_\phi \rangle \langle \chi \rangle \langle \epsilon \rangle^{1/3} k^{-1}$ from forced 64^3 LES using multifractal model at Schmidt number $Sc = 100$ at $Re_\lambda \approx 50$. Both graphics reflect spectra averaged over the interval $20t_o \leq t \leq 70t_o$, after the system had reached a statistically stationary state. Note that no appreciable inertial range exists for the velocity field at this low Reynolds number. Thus, most of the scalar spectrum falls within the viscous-convective range and accordingly exhibits a k^{-1} scaling over most resolved wavemodes, as predicted by Batchelor (1959). Compare with Fig. 8, below.

high Schmidt-number mixing are still incompletely understood, and remain the subject of much debate. These limitations suggest that large-eddy simulation may provide an attractive alternative method to study high Schmidt-number flows, so long as the subgrid model retains substantial physical fidelity. Such simulations would in theory allow significantly higher Taylor-scale Reynolds numbers to be examined, where the existence of an appreciable inertial range in the velocity field would allow better evaluation of passive-scalar energy scaling in both the inertial- and viscous-convective ranges. Importantly, however, an extensive literature search has failed to identify any LES study of passive scalar mixing at Schmidt numbers $Sc \gg 1$. Therefore, a second series of turbulent mixing simulations using multifractal modeling was run at a high Schmidt number ($Sc = 100$), where forced, homogeneous, isotropic turbulence was used to mix the passive scalar. Because a significant separation between the Kolmogorov and Batchelor scales is required to observe the viscous-convective range scaling, all simulations were run at the finer resolution of 64^3. A first set of simulations was made at $Re_\lambda \approx 50$, so that the widest possible scale range existed between the viscous scales of the turbulence and the diffusive scales in the scalar field, yet where the velocity field remained at least modestly turbulent. Figure 7 *(left)* depicts the kinetic energy spectrum $E(k)$ for this simulation, averaged over the interval $20t_o \leq t \leq 70t_o$, after the system had reached a statistically stationary state. It is clear from this graphic that there is no appreciable inertial range in the velocity field, which is thus dominated by viscous forces. The averaged scalar energy spectrum $E_\phi(\mathbf{k})$, compensated by $\langle E_\phi \rangle \langle \chi \rangle \langle \epsilon \rangle^{1/3} k^{-1}$ is depicted in Fig. 7 *(right)*, and clearly displays k^{-1} scaling over most resolved scales in the LES. This provides substantial support for the existence of Batchelor scaling in similar high Schmidt-number flows. A second series of large-eddy simulations was then conducted, at the same high Schmidt number of $Sc = 100$, but also at a substantially higher Reynolds number of $Re_\lambda \approx 150$, by reducing the magnitudes of both the kinematic viscosity and the scalar diffusivity by two orders of magnitude. This provided an inertial range over at least half of the resolved wavemodes in the LES. The simulations again were integrated to over $70t_o$ and both ki-

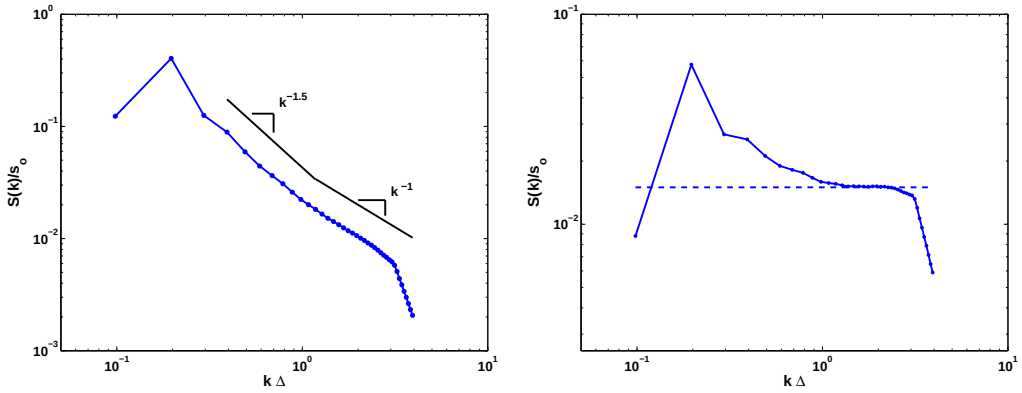

FIGURE 8. Scalar-energy spectra, uncompensated *(left)* and compensated by $\langle E_\phi \rangle \langle \chi \rangle \langle \epsilon \rangle^{1/3} k^{-1}$ *(right)*, from 64^3 LES of passive-scalar mixing at high Reynolds-number $Re_\lambda \approx 150$ and high Schmidt number $Sc = 100$, using multifractal subgrid-scale modeling. The spectra represent averages over period $20t_o \leq t \leq 70t_o$. Due to the presence of inertial range scaling in the velocity field at this higher Reynolds number, the scalar spectrum scales as $\sim k^{-1.5}$ at the larger scales, approximately in agreement with Corrsin and Obukhov, followed by a $\sim k^{-1}$ scaling at smaller scales in accordance with Batchelor (1959). Compare with Fig. 7, above.

netic and scalar energy spectra were averaged over the period of statistical stationarity. Figure 8 shows the scalar energy spectrum $E_\phi(k)$ averaged over the same period, uncompensated *(left)*, and compensated by $\langle E_\phi \rangle \langle \chi \rangle \langle \epsilon \rangle^{1/3} k^{-1}$ *(right)*. The graphic shows clear evidence of two distinct scaling regimes. At the smaller resolved scales, the spectrum exhibits a region of k^{-1} scaling, consistent both with Batchelor's prediction and the results in Fig. 7. However, the scalar spectrum exhibits a second scaling range with a markedly steeper slope of $\sim k^{-1.5}$, between the large forcing scales and the small viscous range. While somewhat below the $k^{-5/3}$ scaling predicted by Obukhov and Corrsin, the results fall squarely within previous experimental and DNS studies examining the scalar energy distribution in the inertial-convective range (Warhaft 2000). The current study therefore has used the multifractal LES methodology to independently evaluate the distribution of scalar energy in high Schmidt- number mixing, and has found support for the existence both of the Batchelor scaling in the viscous-convective range and of Obukhov-Corrsin scaling in the inertial-convective range.

3. Future plans

Future work will focus on establishing the dependence of various scalar mixing statistics on the Reynolds and Schmidt numbers of a given flow. These include normalized scalar variance, the persistence of anisotropy as measured by scalar gradient skewness, the degree of intermittency of the scalar field, and the ratio of mechanical to scalar time scales. Multifractal modeling will then be used to investigate the power spectra of passive scalars mixed in an incompressible axisymmetric jet at high Schmidt number. Finally, reacting flow in an axisymmetric jet will be simulated using LES, with multifractal modeling providing the input parameters to current combustion models that rely on passive-scalar statistics of the resolved and subgrid fields.

Acknowledgments

Discussions with Drs. Volker Gravemeier and Yves Dubief are gratefully acknowledged.

REFERENCES

Antonia, R.A., Chambers, A.J., Britz, D & Browne, L.W. 1986 Organized structures in a turbulent plane jet: topology and contribution to momentum and heat transport. *J. Fluid Mech.* **172**, 211-29.

Batchelor, G. K. 1959 Small-scale variation of convected quantities like temperature in turbulent fluid. *J. Fluid Mech.* **5**, 113-133.

Burton, G. C. 2004 Large-eddy simulation of passive-scalar mixing using multifractal subgrid-scale modeling. *Annual Research Briefs 2004* Center for Turbulence Research, NASA Ames/Stanford Univ.

Burton, G. C. & Dahm, W. J. A. 2005*a* Multifractal subgrid-scale modeling for large-eddy simulation. Part 1: Model development and *a priori* testing. *Phys. Fluids.* **17**, 075111.

Burton, G. C. & Dahm, W. J. A. 2005*b* Multifractal subgrid-scale modeling for large-eddy simulation. Part 2: Backscatter limiting and *a posteriori* evaluation. *Phys. Fluids.* **17**, 075112.

Corrsin, S. 1951 On the spectrum of isotropic temperature fluctuations in isotropic turbulence. *J. Appl. Phys.* **22**, 469.

Frederiksen, R. D., Dahm, W. J. A. & Dowling, D. R. 1997 Experimental assessment of fractal scale similarity in turbulent flows. Part 3. Multifractal scaling. *J. Fluid Mech.* **338**, 127-155.

Gollub, J.P., Clarke, J., Gharib, M., Lane, B. & Mesquita,O.N. 1991 Fluctuations and transport in a stirred fluid with a mean gradient. *Phys. Rev. Lett.* **67**, 3507-3510.

Miller, P.L. & Dimotakis, P.E. 1996 Measurements of scalar power spectra in high Schmidt number turbulent jets. *J. Fluid Mech.* **308**, 129-146.

Moin, P., Squires, K. Cabot, W & Lee, S. 1991 A dynamic subgrid-scale model for compressible turbulence and scalar transport. *Phys. Fluids A* **3**, 2746-2757.

Mydlarski, L. & Warhaft, Z. 1998 Passive scalar statistics in high Peclet-number grid turbulence. *J. Fluid Mech.* **358**, 135-175.

Obukhov, A.M. 1949 The structure of the temperature field in a turbulent flow. *Izv. Nauk. SSSR. Geophys.* **13**, 58-69.

Overholt, M. R. & Pope, S. B. 1996 Direct numerical simulation of a passive scalar with imposed mean gradient in isotropic turbulence *Phys. Fluids* **8**, 3128-3148.

Prasad, R. R., Meneveau, C. & Sreenivasan, K. R. 1988 The multifractal nature of the dissipation field of passive scalars in fully turbulent flows. *Phys. Rev. Lett.* **61**, 74-77.

Pullin, D.I. 2000 A vortex-based model for the subgrid flux of a passive scalar. *Phys. Fluids* **12**, 2311-2319.

Warhaft, Z. 2000 Passive scalars in turbulent flows. *Ann. Rev. Fluid Mech.* **32**, 203-240.

Yeung, P. K., Donzis, D. A & Sreenivasan, K. R. 2005 High-Reynolds-number simulation of turbulent mixing. *Phys. Fluids* **17**, 081703.

Yeung, P. K., Xu, S., Donzis, D. A & Sreenivasan, K. R. 2004 Simulations of three-dimensional turbulent mixing for Schmidt numbers of the order 1000. *Flow, Turb. Combust.* **72**, 333-347.

Yeung, P. K., Xu, S. & Sreenivasan, K. R. 2002 Schmidt number effects on turbulent transport with uniform mean scalar gradient. *Phys. Fluids* **14**, 4178-4191.